ADVANCED ENERGY MATERIALS
www.advmat.de

Nanostructured Fe_3O_4/SWNT Electrode: Binder-Free and High-Rate Li-Ion Anode

By *Chunmei Ban, Zhuangchun Wu, Dane T. Gillaspie, Le Chen, Yanfa Yan, Jeffrey L. Blackburn,* and *Anne C. Dillon**

Rechargeable Li-ion batteries are currently being explored for high-power applications such as electric vehicles. However, in order to deploy Li-ion batteries in next-generation vehicles, it is essential to develop electrodes made from durable, nontoxic, and inexpensive materials with a high charge/discharge rate and a high reversible capacity. Transition metal oxides such as Fe_3O_4, Fe_2O_3, MoO_3, and Co_3O_4 [1–5] are capable of Li^+ insertion/extraction in excess of 6 Li^+ per formula unit, resulting in a significantly larger reversible capacity than commercially employed graphite. In contrast to the intercalation mechanism that occurs for graphite, the transition metal oxides are reduced in a conversion reaction to small metal clusters with the oxygen reacting with Li^+ to form Li_2O.[1,2,6] This usually leads to large volume expansion and destruction of the structure upon electrochemical cycling, especially at high rate. Hence, optimizing particle size and mixing the particles with various carbon additives have been employed to improve the reversible capacity and rate capability of metal oxide electrodes.[6–13] Among the transition metal oxides, Fe_3O_4 is both nontoxic and abundant (inexpensive) and is thus considered one of the most promising electrode materials.[2,14,15] However, a truly durable high-rate capability and a high capacity for metal oxide based electrodes including Fe_3O_4 have not yet been achieved.

To achieve high-rate capability and high capacity using metal oxide nanoparticles mixed with carbon materials, there are three key issues that must be considered: i) the size of the nanoparticles must be optimized such that rapid Li-ion diffusion and reaction with metal oxide nanoparticles are achieved,[8–11] ii) an optimized carbon matrix must be developed that ensures both electrical conductivity and good thermal conductivity (to improve heat-dissipation), and iii) the conductive additive must maintain a flexible and strong matrix that accommodates large volume changes. In most conventional electrodes, metal oxide nanoparticles are directly mixed with a carbon additive and a binder to help maintain electrical conductivity, and the large volume expansion then results in mechanical degradation of the electrode when cycled at high rate.

Here we employ the unique properties of highly crystalline and long single-walled carbon nanotubes (SWNTs)[16] to simultaneously address all of the three key issues with a simple two-step process to synthesize Fe_3O_4 nanoparticles embedded uniformly in an interconnected "SWNT net." Furthermore, no polymer binder is required to maintain electrical conductivity. The electrodes contain 95 wt% active material with only 5 wt% SWNTs as the conductive additive (typical electrodes contain 80 wt% active material and 20 wt% conductive and binder additives). Most importantly, by using these binder-free electrodes, we have demonstrated a high reversible capacity of 1000 mAh g^{-1} (~2000 mAh cm^{-3}) at C rate as well as high-rate capability and stable capacities of 800 mAh g^{-1} at 5C (both for over 100 deep charge/discharge cycles) and ~600 mAh g^{-1} at 10C. Raman spectroscopy suggests that this remarkable rate capability is achieved because the Fe_3O_4 nanoparticles are actually bound to the flexible nanotube net. We also believe that this fabrication method may be employed for other active materials to achieve a binder-free, high-rate, and durable electrode.

The FeOOH nanorods, employed as a precursor in the electrode fabrication process, have a width of ~50 nm, length of ~250 nm, and thickness of ~20 nm and are formed with a simple hydrothermal process. X-ray diffraction (XRD) spectra of the as-prepared nanorods and reference α-FeOOH phase (goethite, JCPDS 81-0463) are shown in Figure 1a. All of the reflection peaks can be indexed to the tetragonal α-FeOOH phase. Next we created Fe_3O_4 nanoparticles embedded in an interconnected SWNT network using FeOOH nanostructures and SWNTs as precursors for a vacuum-filtration and subsequent annealing process. We found that annealing the FeOOH nanorods without SWNTs to 450 °C in an argon atmosphere leads to a mixture of α-Fe_2O_3 (hematite) and Fe_3O_4 (magnetite) as indicated by the XRD patterns in Figure 1b. The peaks marked with * are indexed to the Fe_3O_4 phase (JCPDS 88-0315) and the remainder of the diffraction peaks are indexed to α-Fe_2O_3, (JCPDS 33-0664). In contrast, annealing FeOOH nanorods mixed with 5 wt% SWNTs at 450 °C in an argon atmosphere leads to the complete reduction of FeOOH to Fe_3O_4, as indicated in Figure 1c. It is therefore evident that the SWNTs actually facilitate the formation of Fe_3O_4 nanoparticles, enabling excellent Fe_3O_4 nanoparticle/SWNT electronic and mechanical contact, which is further confirmed by the Raman spectroscopy analysis discussed later.

The elegant morphology of the Fe_3O_4 nanorods embedded uniformly in the SWNT net is clearly depicted in the scanning electron microscope (SEM) image of Figure 2a. Figure 2b displays

[*] Dr. A. C. Dillon, Dr. C. Ban, Dr. Z. Wu, Dr. D. T. Gillaspie, Dr. J. L. Blackburn
Materials and Chemical Science Center
National Renewable Energy Lab
1617 Cole Boulevard, Golden, Colorado 80401 (USA)
E-mail: Anne.Dillon@nrel.gov
Dr. L. Chen, Dr. Y. Yan
National Center for Photovoltaics
National Renewable Energy Lab
1617 Cole Boulevard, Golden, Colorado 80401 (USA)

DOI: 10.1002/adma.200904285

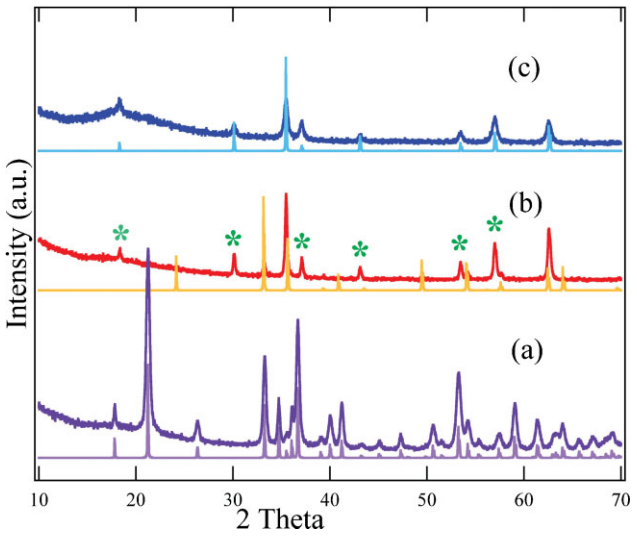

Figure 1. XRD patterns of a) hydrothermal product, α-FeOOH (JCPDS 81-0463), b) annealing the as-prepared sample under Ar atmosphere to 450 °C, Fe_2O_3 (JCPDS 33-0664), c) the nanostructured SWNT/Fe_3O_4 electrode created by annealing the vacuum filtration product to 450 °C, Fe_3O_4 (JCPDS 88-0315).

a colorized cross-sectional SEM image of the same electrode, with the Fe_3O_4 nanorods exhibited in yellow/blue and the high-aspect-ratio (narrow and long) SWNT bundles in white. The nanoscale Fe_3O_4/SWNT electrode is very porous. The removal of H_2O and reduction of Fe (III) to Fe (II) that occurs in the annealing process likely enables the formation of the porous network. This porosity promotes the diffusion of Li ions in the electrode and enables the achievement of durable high-rate capability.[17]

Charge transfer between the Fe_3O_4 nanorods and SWNTs is confirmed by Raman spectroscopic analyses, depicted in Figure 3. Raman spectra of SWNT materials are composed of resonantly enhanced tangential bands between 1500–1600 cm^{-1} (G-bands) as well as a broad band at ~1350 cm^{-1} attributed to a convolution of the disorder-induced band (D-band) of carbon impurities and the D-band of the SWNTs themselves. The carbon tangential vibrations are strong first-order bands, consisting of six components with $2A + 2E_1 + 2E_2$ symmetries arising from curvature-induced splitting of the tangential E_{2g} mode of graphite.[18] The line shapes and widths of these modes vary significantly, depending on how close the laser excitation energy is to the nanotube resonance and whether the nanotube is semiconducting or metallic. Typically the semiconducting bands are fit with multiple Lorentzians to describe the six Raman active modes, and the metallic tubes are fit with only two peaks, a Lorentzian line shape describing the dominant higher-frequency feature, and a Breit–Wigner–Fano (BWF) line describing the dominant lower frequency feature.[19]

The G-band features in the spectra of the pure SWNTs indicate that both semiconducting and metallic nanotubes are present in the purified sample. Also, the intensity of the D-band in the purified sample suggests the presence of some non-nanotube carbon. Changes in the Raman spectrum of the SWNTs in the electrode after annealing to 450 °C are clearly observed. The

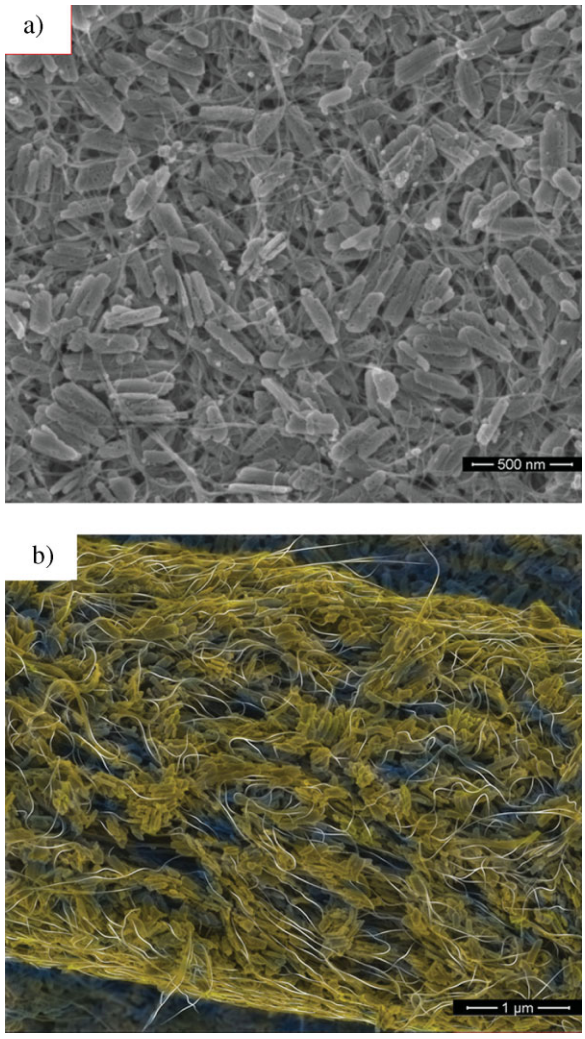

Figure 2. SEM images of the nanostructured Fe_3O_4 electrode a) surface and b) cross-section with colorization for enhanced visualization.

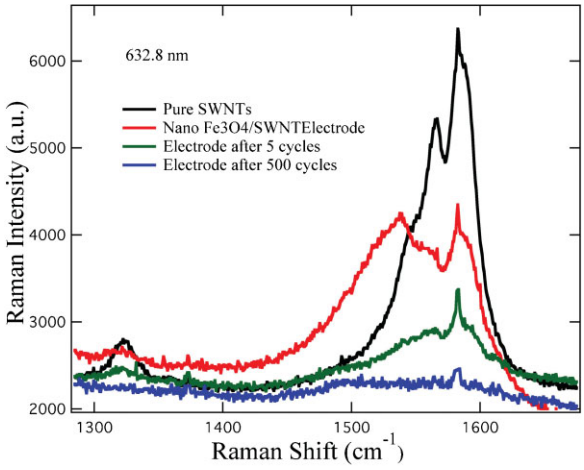

Figure 3. Raman spectra of pure SWNTs, the nanostructured Fe_3O_4/SWNT electrode (annealed to 450 °C), and cycled electrodes.

loss of intensity of the D-band relative to the G-bands is consistent with the oxidation of residual non-nanotube carbon.[19] The change in shape of the G-bands and the large shift/increase in the dominant low-frequency feature suggests significant charge transfer between the nanotubes and the Fe_3O_4 nanorods. The magnitude of the intensity increase coupled with the shift of the lower frequency line from ~1554 to 1538 cm^{-1} suggests very strong charge transfer and that the SWNTs may actually be bound to the iron oxide nanorods. (This will be the subject of a future detailed Raman and nuclear magnetic resonance investigation.) The quenching of the Raman lines in the cycled electrodes is attributed to the irreversible insertion of Li^+ into the SWNT bundles between 3 and 0.005 V and is consistent with previous Raman studies examining ion intercalation in SWNTs.[18]

Most importantly, the binder-free Fe_3O_4/SWNT anode (nano) exhibits excellent electrochemical performance, which is characterized using galvanostatic cycling in a coin cell with Li metal as the negative electrode. We attribute the significantly enhanced performance to our two-step hydrothermal/annealing process that ensures anomalous physical contact/charge transfer between the Fe_3O_4 nanorods and SWNTs. However, in order to conclusively demonstrate this, we have prepared anodes in which 5 μm Fe_3O_4 particles (from Aldrich) were mixed with 10 wt% SWNTs and prepared with our two-step process (micro2) as well as a pure SWNT electrode (SWNT), and finally a conventional electrode fabricated with carbon black (CB) and polyvinylidene fluoride (PVDF) binder using the 5 μm Fe_3O_4 particles (micro1). The Li^+ insertion/extraction process in the first two cycles is depicted in Figure 4a for each of the above electrodes. This comparison enables us not only to examine the effect of various electrode preparation methods but also the effect of Fe_3O_4 particle size.

The voltage of the pure SWNT electrode (SWNT) rapidly reaches a plateau at 1.0 V before a smooth and long slope (Li^+ insertion into SWNT bundles[20]) is observed. A solid electrolyte interphase (SEI) formation on the large surface of SWNTs causes the irreversible capacity observed around 1.0 V. During charging, there is no obvious plateau below 0.2 V where Li^+ intercalation in graphitic carbons is generally observed.[20] As previously noted, the Raman data in Figure 3 are consistent with irreversible Li-ion insertion in the SWNT bundles between 3 and 0.005 V. For the first discharge curves of micro1, micro2, and nano, a well-defined plateau is observed at 0.8 V and is attributed to the reduction of Fe_3O_4 into Fe (II) and Fe (0).[1] Compared to the potential curves of the microstructured Fe_3O_4 electrodes (micro1 and micro2), the voltage profile of the first discharge curve of the nanostructured Fe_3O_4 electrode (nano) has a different behavior before the conversion plateau at 0.8 V. Specifically, a smooth slope with a plateau-like step at 1.2 V is observed in the first discharge of the nanostructured Fe_3O_4 electrode. Lithium intercalation in the nanostructured Fe_3O_4 before the conversion reaction, leading to a change of crystalline structure, accounts for this discharge behavior and was previously reported for nanostructured Fe_2O_3.[10,11] Note also that Li^+ consumption attributed to the formation of an SEI layer on the SWNTs explains the short plateau around 1.0 V observed for both nano and micro2. Because of the irreversible Li^+ loss associated with the SWNT SEI formation, these electrodes both have higher first discharge capacities than the theoretical capacity of Fe_3O_4 (expected in the reduction of

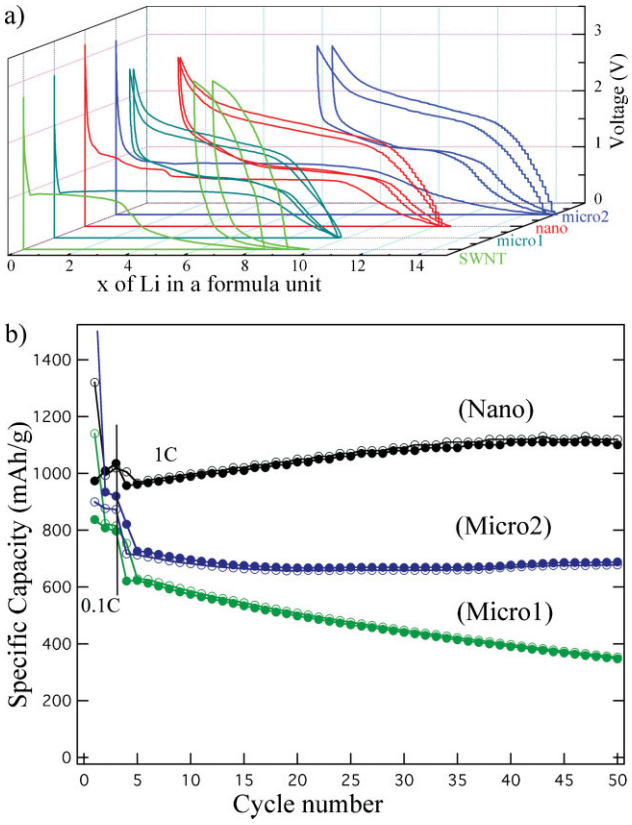

Figure 4. a) Voltage-composition curves for various electrodes cycled between 0.005 and 3 V at 0.1C rate for a pure SWNT electrode (SWNT), a conventional micrometer-scale Fe_3O_4 electrode made with commercial 5 μm Fe_3O_4 and AB and PVDF (micro1), a micrometer-scale Fe_3O_4 electrode made with commercial 5 μm Fe_3O_4 and 10 wt% SWNTs (micro2), and our nanostructured Fe_3O_4 electrode fabricated with 10 wt% SWNTs (nano). b) Comparison of specific capacity versus cycle number for various Fe_3O_4 electrodes at C rate: nano, micro1, and micro2.

Fe_3O_4 by 8 Li^+). Although an identical fabrication method was used, we note that the nanostructured Fe_3O_4 electrode has a higher initial Coulombic efficiency (~75%) than that of the microstructure Fe_3O_4 electrode (~55%). Thus we believe that amphorization of the micrometer-sized Fe_3O_4 also contributes to a significant irreversible capacity for the micrometer-sized Fe_3O_4 electrode (micro2). After the first discharge, the nanostructured Fe_3O_4 electrode stabilizes at the theoretical capacity, and a similar voltage profile to both of the micrometer-sized Fe_3O_4 electrodes is observed, indicating a similar conversion reaction during charge/discharge.

The subsequent 50 cycles were performed at a higher current rate of 1C (8 Li^+ per formula unit in 1 h). Figure 4b shows the Li^+ insertion and extraction capacities per unit mass of Fe_3O_4 versus cycle number. The capacity of the conventional Fe_3O_4 electrode (micro1) deteriorates after the first cycle and loses ~50% of the initial charge capacity after only 50 cycles. Volume expansion due to the conversion reaction compromises the structural integrity of conventional electrodes made with CB and PVDF and results in rapid capacity fade. Although the capacity of the microstructured Fe_3O_4 electrode fabricated with SWNTs with our new method (micro2) decreases to ~600 mAh g^{-1} upon initial

cycling at 1C rate, the capacity then remains constant at 600 mAh g^{-1} for 50 cycles. This demonstrates that our electrode preparation method greatly improves the cycling performance even for electrodes utilizing micrometer-sized particles and thus may be very valuable to the improvement of all battery electrode technologies.

The best result is, of course, obtained for the nanostructured Fe_3O_4 electrode. After the first three cycles at the low rate of 0.1C, the capacity remains constant at 1000 mAh g^{-1} (~2000 mAh cm^{-3}) and then slightly increases while cycling at 1C rate. The rise in capacity is not surprising for the nanostructured Fe_3O_4 electrode, although it is rarely observed when an intercalation mechanism is occurring. (We note that Tarascon's group[21] has proposed that a gel-like film resulting from decomposition of the electrolyte at low voltage plays a crucial role in this capacity increase.) Exceptionally, the intrinsic mechanical/electronic properties of SWNTs coupled with the "flexible conductive SWNT net" (fabricated here) allow for volume expansion/contraction and also improve the electrical and thermal conductivity. Specifically, we found that the resistance is reduced from 1500 Ω sq^{-1} for the conventional Fe_3O_4 electrode with CB and PVDF (micro1) to 50 Ω sq^{-1} for the nanostructured Fe_3O_4 electrode with only 5 wt% SWNTs (nano).

The remarkably high-rate capability of the nanostructured Fe_3O_4/SWNT electrode is demonstrated in Figure 5a. The electrodes were fabricated with various ratios of nanostructured Fe_3O_4 and SWNTs (5 wt% SWNTs, 10 wt% SWNTs, and 30 wt% SWNTs) and were tested to establish the effect of electrode composition on high-rate capability. The best performance is obtained by using only 5 wt% SWNTs. This cell retains a capacity of 550 mAh g^{-1} at 10C (8 Li^+ per formula unit in 6 min) after 60 cycles of variable charging rate, superior to the cell with 30% SWNTs, which only retains a capacity of 200 mAh g^{-1}. The SEI formation for the increased SWNT loading explains the higher irreversible capacity. Although the integrity of the electrodes may be affected by using very low SWNT loadings, the data in Figure 5a suggests that there is an optimal ratio between SWNT loading and the nanostructured Fe_3O_4 active material. At high SWNT loadings, the nanotubes will agglomerate into larger bundles due to very strong van der Waals interactions between the tubes decreasing the flexibility and connectivity of the nanotube network.[18] Also, the conductivity decreases in the SWNT networks as the bundle diameter increases,[22,23] which accounts for the inferior rate capability of the electrodes with higher SWNT loadings. We also tested the durability of a nanostructured Fe_3O_4 electrode with 5 wt% SWNTs at a constant high rate of 5C (4360 mA g^{-1}). The data is shown in Figure 5b and represents deep charge and discharge cycles in 12 min without any voltage-holding step. The capacity at 5C rate is 850 mAh g^{-1} in the initial cycle with a very slow capacity fade to 790 mAh g^{-1} after 60 cycles.

In summary, we report a simple two-step process, hydrothermal synthesis, and vacuum filtration to fabricate binder-free, high-rate capability Li-ion anodes from nontoxic and abundant elements. Utilizing Fe_3O_4 nanorods as the active Li^+ storage material and 5 wt% SWNTs as the conductive additive, our electrodes reach the theoretical reversible capacity of 1000 mAh g^{-1} (~2000 mAh cm^{-3}) at C rate and also exhibit high-rate capability and stable capacities of 800 mAh g^{-1} at 5C and ~600 mAh g^{-1} at 10C. Raman spectroscopy indicates that the anomalous rate capability for this high-volume-expansion material is attributed to charge transfer, perhaps indicative of a physical bond between the flexible SWNT conductive net and the iron oxide nanoparticles. Finally this new method can be easily adapted to fabricate other high-rate capability anodes and cathodes.

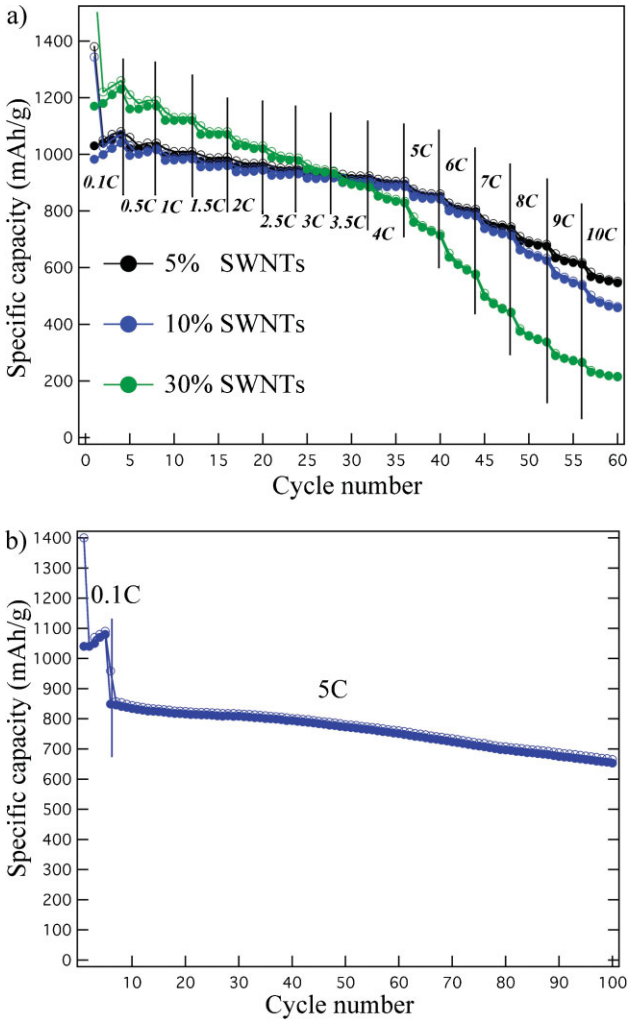

Figure 5. a) Rate capability for the nanostructured Fe_3O_4 electrodes with different SWNT contents. The cells were cycled between 0.005 and 3 V with increasing rates. b) Cycling stability of the nanostructured Fe_3O_4 electrode (5 wt% SWNTs) at a high rate of 5C (4630 mA g^{-1}).

Experimental

Electrode Fabrication: FeOOH nanorods employed as a precursor to make iron (II, III) oxide (Fe_3O_4) electrodes were synthesized by a hydrothermal process. $FeCl_3$ (0.405 g) was dissolved in distilled water and added to NaOH (0.400 g) solution. The mixture was stirred to form a homogeneous gel before it was transferred into a Teflon-lined stainless steel autoclave. The reaction was maintained at 160 °C for 24 h. After cooling to room temperature, the product was rinsed with distilled water and dried at 80 °C under vacuum. Raw material containing SWNTs was produced by the laser vaporization method [24]. Significant agglomerations

of amorphous and nanocrystalline carbon as well as metal nanoscale catalyst particles (Ni, Co) in the as-produced raw SWNTs were removed by an HNO_3 reflux/air oxidation procedure [25]. A known vacuum filtration method [26] was used to fabricate the nanostructured Fe_3O_4/SWNT electrode. FeOOH nanorods from the hydrothermal process and purified SWNTs were suspended in sodium dodecyl sulfate (SDS) solution and sonicated for 15 min before vacuum filtration. The resulting film was rinsed with deionized water and then transferred to Cu foil. The electrode was then baked in an argon atmosphere at 450 °C for 1 h. The conventional Fe_3O_4 electrodes were made by mixing the Fe_3O_4 (5 μm particle size, purchased from Aldrich) with acetylene black (Super P, from TIMCAL) and polyvinylidene fluoride (HSV 900, from Kynar) at a weight ratio of 80:8:12 and then vacuum dried at 120 °C for 8 h.

Characterization: The morphology and distribution of Fe_3O_4 in the nanotube net were investigated by a SEM (FEI NOVA 630). XRD data were collected on a powder Scintag XRD operating at 45 kV and 36 mA and using Cu-Kα radiation. Raman spectroscopy was performed using 632.8 nm (1.96 eV) laser excitation. The back-scattered light was analyzed with a Jobin Yvon 270M spectrometer equipped with a liquid-nitrogen-cooled Spectrum One CCD and holographic notch filters. Averaging three 30 s scans was sufficient to obtain high intensity, well-resolved Raman spectra. 2025 Coin cells were assembled in an argon-filled dry box using the binder-free electrode as the positive electrode and Li metal as the negative electrode. A Celgard separator 2325 and 1 M $LiPF_6$ electrolyte solution in 1:1 w/w ethylene carbonate/diethyl carbonate (purchased from Novolyte) were used to fabricate the coin cells.

Acknowledgements

C. Ban and Z. Wu contributed equally to experimental and scientific development. D. T. Gillaspie contributed to the electrochemical testing and scientific development. L. Chen and Y. Yan performed the SEM imaging. J. L. Blackburn contributed to SWNT synthesis. A. C. Dillon performed Raman spectroscopy and supervised the work. This work was funded by the U.S. Department of Energy under subcontract number DE-AC36-08GO28308 through the DOE Office of Energy Efficiency and Renewable Energy Office of the Vehicle Technologies Program. We thank Professor Mildred S. Dresselhaus for useful discussions regarding the Raman spectroscopy and Alfred Hicks for the color-enhanced SEM images.

Received: December 15, 2009
Revised: January 18, 2010
Published online: May 3, 2010

[1] P. Poizot, S. Lauruelle, S. Grugeon, L. Dupont, J.-M. Tarascon, *Nature* **2000**, *407*, 496.
[2] P. L. Taberna, S. Mitra, P. Poizot, P. Simon, J.-M. Tarascon, *Nat. Mater.* **2006**, *5*, 567.
[3] Y.-S. Hu, Y.-G. Guo, W. Sigle, S. Hore, P. Balaya, J. Maier, *Nat. Mater.* **2006**, *5*, 713.
[4] P. Balaya, H. Li, L. Kienle, J. Maier, *Adv. Funct. Mater.* **2003**, *13*, 621.
[5] N. A. Chernova, M. Roppolo, A. C. Dillon, M. S. Whittingham, *J. Mater. Chem.* **2009**, *19*, 2526.
[6] S. H. Lee, Y. H. Kim, R. Deshpande, P. A. Parilla, E. Whitney, D. T. Gillaspie, K. M. Jones, A. H. Mahan, S. B. Zhang, A. C. Dillon, *Adv. Mater.* **2008**, *20*, 3627.
[7] Y. S. Jung, S. Lee, D. Ahn, A. C. Dillon, S. H. Lee, *J. Power Sources* **2009**, *188*, 286.
[8] S. Grugeon, S. Larruelle, R. Herrera-Urbina, L. Dupont, P. Poizot, J.-M. Tarascon, *J. Electrochem. Soc.* **2001**, *148*, A285.
[9] F. Jiao, J. Bao, P. G. Bruce, *Solid State Lett.* **2007**, *10*, A264.
[10] D. Larcher, C. Masquelier, D. Bonnin, Y. Chabre, V. Masson, J.-B. Leriche, J.-M. Tarascon, *J. Electrochem. Soc.* **2003**, *150*, A133.
[11] D. Larcher, D. Bonnin, R. Cortes, I. Rivals, L. Personnaz, J.-M. Tarascon, *J. Electrochem. Soc.* **2003**, *150*, A1643.
[12] B. T. Hang, S. Okada, J. Yamaki, *J. Power Sources* **2008**, *178*, 402.
[13] V. L. Pushparaj, M. M. Shaijumon, A. Kumar, S. Murugesan, L. Ci, R. Vajtai, R. J. Linhardt, O. Nalamasu, P. M. Ajayan, *Proc. Natl. Acad. Sci. USA* **2007**, *104*, 13574.
[14] Z.-M. Cui, L.-Y. Jiang, W.-G. Song, Y.-G. Guo, *Chem. Mater.* **2009**, *21*, 1162.
[15] L. Wang, Y. Yu, P. C. Chen, D. W. Zhang, C. H. Chen, *J. Power Sources* **2008**, *183*, 717.
[16] R. H. Baughman, A. A. Zakhidov, W. A. de Heer, *Science* **2002**, *297*, 787.
[17] X. Wang, L. Gao, H. Zheng, M. Ji, C. Tang, T. Shen, Z. Zhang, X. Wang, *J. Mater. Chem.* **2004**, *14*, 905.
[18] R. Saito, G. Dresselhaus, M. S. Dresselhaus, *Physical Properties of Carbon Nanotubes*, Imperial College Press, London **1998**.
[19] A. C. Dillon, M. Yudasaka, M. S. Dresselhaus, *J. Nanosci. Nanotechnol.* **2004**, *407*, 691.
[20] E. Frackowiak, F. Beguin, *Carbon* **2002**, *40*, 1775.
[21] S. Laruelle, S. Grugeon, P. Poizot, D. S. Molle, L. Dupont, J.-M. Tarascon, *J. Electrochem. Soc.* **2002**, *149*, A627.
[22] P. E. Lyons, S. De, F. Blighe, V. Nicolosi, L. F. C. Pereira, M. S. Ferreira, J. N. Coleman, *J. Appl. Phys.* **2008**, *104*, 044302.
[23] P. N. Nirmalraj, P. E. Lyons, S. De, J. N. Coleman, J. J. Boland, *Nano Lett.* **2009**, *9*, 3890.
[24] A. C. Dillon, P. A. Parilla, J. L. Alleman, J. D. Perkins, M. J. Heben, *Chem. Phys. Lett.* **2000**, *316*, 13.
[25] A. C. Dillon, T. Gennett, K. M. Jones, J. L. Alleman, P. A. Parilla, M. J. Heben, *Adv. Mater.* **1999**, *11*, 1354.
[26] Z. C. Wu, Z. H. Chen, X. Du, J. M. Logan, J. Sippel, M. Nikolou, K. Kamaras, J. R. Reynolds, D. B. Tanner, A. F. Hebard, A. G. Rinzler, *Science* **2004**, *305*, 1273.